ACS Photonics

Article

pubs.acs.org/journal/apchd5

Self-Assembled Spherical Supercluster Metamaterials from Nanoscale Building Blocks

Vladimir A. Turek,[†,§] Yan Francescato,[‡,§] Paolo Cadinu,[†,§] Colin R. Crick,[†] Laura Elliott,[†] Yiguo Chen,[‡,⊥] Viktoria Urland,[†] Aleksandar P. Ivanov,[†] Leonora Velleman,[†] Mingui Hong,[⊥] Ramon Vilar,[†] Stefan A Maier,[*,‡] Vincenzo Giannini,[*,‡] and Joshua B. Edel[*,†]

[†]Department of Chemistry, and [‡]Department of Physics, Imperial College London, South Kensington Campus, London, SW7 2AZ, United Kingdom

[⊥]Department of Electrical and Computer Engineering, National University of Singapore, 4 Engineering Drive 3, Singapore 117576, Singapore

Supporting Information

ABSTRACT: We report on a simple, universal, and large-scale self-assembly method for generation of spherical superclusters from nanoscopic building blocks. The fundamentals of this approach rely on the ultrahigh preconcentration of nanoparticles (NP) followed by using either emulsification strategies or alternatively multiphase microfluidic microdroplets. In both cases drying of the NP droplets yields highly spherical self-assembled superclusters with unique optical properties. We demonstrate that the behavior of these spheres can be controlled by surface functionalization before and after the self-assembly process. These structures show unique plasmonic collective response both on the surface and within the supercluster in the visible and infrared regions. Furthermore, we demonstrate that these strong, tunable optical modes can be used toward ultrasensitive, reproducible, surface-enhanced spectroscopies.

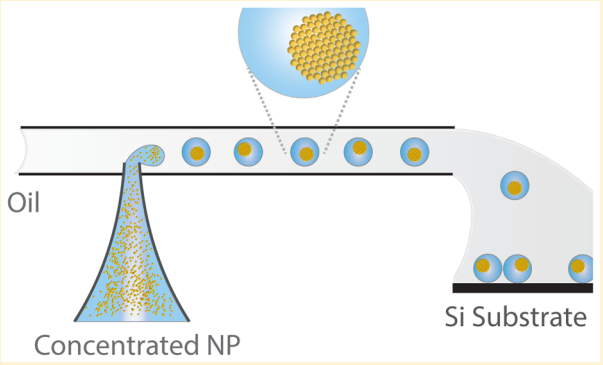

KEYWORDS: *surface-enhanced Raman spectroscopy, self-assembly, superclusters, metamaterials, nanoparticles*

Controlled bottom-up assembly of nanoscale building blocks into hierarchical superstructures is one of the most hotly pursued topics in nanotechnology.[1−3] From medicine,[4] to materials science,[5] electronics,[6] and catalysis,[7] the ability to reproducibly assemble engineered macroscopic structures from specifically chosen nanoscopic objects has the potential to revolutionize an enormous range of fields. An extensive body of literature exists on different strategies to achieve self-assembly;[8−10] however despite this, the field is still in its infancy. Important problems arise with attempts to control the self-assembly process. For example, although it is possible to use a template to achieve controlled 2D[11] or even 3D[12] self-assembly of nanoparticles (NPs), most templates have specificity to certain types of particles; examples include thiolated templates being selective to gold/silver NP adsorption, while a liquid−liquid interface is selective to larger particles.[13,14] Furthermore, more advanced self-assembly techniques that take advantage of surface functionalization of the NPs and/or templates to interact in a certain way for the purposes of achieving precise control of the assembly often negate one of the most important benefits that such structures offer, that is, the ability to control the functionality of the nanoscopic building blocks. Of particular interest are spherical colloidal crystals, which have attracted a great deal of attention recently due to their unique and tunable optical properties[15,16] and have even been proposed as anodes in lithium ion batteries.[17] Fabrication of such structures has been demonstrated with predominantly nonmetallic building blocks (photonic crystals) in which the van der Waals forces remain low enough to prevent irreversible aggregation from taking place during the drying process.[18−21] Generation of spherical colloidal crystals with plasmonic building blocks however is made more challenging due to the greater propensity of metallic particles to aggregate. This can be overcome either by using small particles (>10 nm)[22−24] or by sterically stabilizing the particles,[25−27] allowing much higher concentrations to be accessible without inducing irreversible aggregation during the assembly process. However, this has the drawback of passivating the surface such that postfunctionalization becomes nontrivial. Given the vast applications in photonics that such structures hold when composed of materials that are otherwise optically mundane, the facile introduction of plasmonic materials may open exciting new directions in sensing and

Received: July 22, 2015
Published: November 19, 2015

DOI: 10.1021/acsphotonics.5b00408
ACS Photonics 2016, 3, 35−42

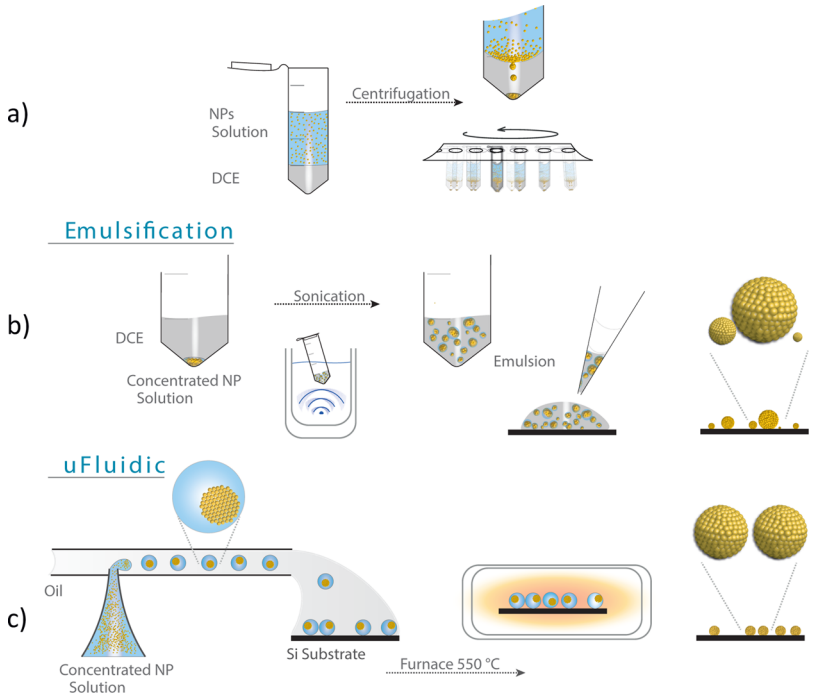

Figure 1. Schematic describing the self-assembly of superclusters. (a) Upon centrifugation of aqueous NPs in the presence of a higher density organic phase (for example 1,2-dichloroethane (DCE)), a high-density aqueous phase is formed at the bottom of the centrifuge tube. (b) When the supernatant aqueous phase is subsequently removed and the resulting mixture sonicated, a water-in-oil emulsion is formed, the aqueous microdroplets possessing a large number of NPs. Due to the fact that the NPs remain unaggregated in the droplets, evaporation of the emulsion leads to a gradual redistribution of the particles' arrangement to adopt the shape of the evaporating droplets, leading to uniform superclusters. (c) Droplets of different sizes, containing a concentrated NP solution, are achieved varying the flow rate of the oil. When the aqueous phase contained in each droplet evaporates, the NPs collapse into sphere. A baking step is required to fully complete the drying process.

metamaterials research. There is therefore a need to introduce additional techniques that are able to generate hierarchical assemblies from a wide selection of building blocks, in a controlled manner that does not limit the particles' functionality.[28]

We have recently reported on a facile and near-universal self-assembly of NPs into a high-density aqueous phase in which the NP concentration is increased to the point where the aqueous phase begins to adopt drastically altered physical properties and the interparticle separation can be controlled in three dimensions through modulation of the electrostatic repulsion between the particles.[29] We build on this concept by developing controlled self-assembly methods that can be achieved with high-concentration NPs in combination with either emulsion generation[30,31] and/or multiphase microfluidic droplets.[31−33] The high NP to liquid volume ratio means that upon drying of the high-density solutions, highly ordered spherical NP superclusters can be quickly and easily formed. The fact that the particles remain unaggregated in the high-density solution leads to self-reorganization of the NPs' arrangement upon drying to adopt the same geometry as that of the evaporating solution; in this instance the spherical geometry was preferred in all cases. Importantly, the self-reorganization of the particles is true of any particle size/shape/composition, as long as the particles remain unaggregated in the high-density solution. This means that even an extremely polydisperse sample or one that has been carefully designed with multiple building blocks will also adopt similar superstructures. Furthermore, this technique does not directly rely on the functionality of the particles (e.g., even aggregation-prone citrate-stabilized gold particles provide sufficient stabilization in the high-density solution), which readily allows for the postfunctionalization of particles or the inclusion of multiple different functionalities in a controlled manner within the same superstructure.

Such structures open up novel avenues for fabrication of metamaterials with unique and tunable optical properties.[34,35] This is demonstrated here by studying experimentally and numerically the near- and mid-IR optical properties of variously sized colloids. Remarkably, these structures support a new kind of collective plasmon supermodes. These strong optical resonances sustain large local field enhancements, which can be harvested for molecular spectroscopy, as the ordered geometry makes it possible to localize the field in hundreds of small gaps. The enhancements obtained in the gaps are similar to the case of a simple dimer, approaching 3 orders of magnitude.[36] In addition, these "metaparticle" structures are extremely promising in order to realize negative refraction metamaterials.[37,38] Here we present as a proof of principle the chemical sensing of trace levels of malachite green (MGITC) using the clusters as surface-enhanced Raman spectroscopy (SERS)-active substrates, which is made possible due to the strong resonant collective mode found throughout the core of the superclusters.

Upon centrifugation of an aqueous NP solution in the presence of a denser organic phase, a high-density droplet can be generated at the bottom of the vial (Figure 1a), which consists of an aqueous phase and concentrated and importantly nonaggregated NPs.[29] These highly concentrated droplets can be converted to three-dimensional hierarchical superclusters by removal of the initial aqueous phase and sonicating (Figure 1b). This results in water-in-oil emulsion microdroplets being

DOI: 10.1021/acsphotonics.5b00408
ACS Photonics 2016, 3, 35−42

formed, which contain a large number of NPs. The relatively long time scales (minutes) for this emulsion to separate back out into the two distinctive phases mean that upon drying of the emulsion, the NPs will rearrange to adopt the gradually reducing droplet volume, thereby generating superclusters of spherical morphology made with the starting NPs. Although emulsification is a rapid process, the dimensions of the clusters are ultimately governed by the distribution of the generated emulsion droplets. Alternatively, microfluidics can be used to precisely control the droplet dimensions[39−41] and hence ultimately the colloid dimensions (Figure 1c) simply by tuning the ratio between the flow rates of the aqueous phase containing concentrated NPs and the organic phase. Within the context of this article both sonication and microfluidic routes are explored.

Microfluidic substrates were fabricated from polydimethylsiloxane (PDMS) and glass (SI Figure S1) using a simple T-junction geometry consisting of both a quartz pipet and PDMS channel as previously described.[42] The channel height and width were 100 μm, respectively. Droplets containing concentrated NP solutions were generated by introducing the NPs as prepared in Figure 1a into the pipet having an internal diameter ranging between 2 and 30 μm (Figure 1c). The dense NP solution was injected in the microfluidic channel while flowing the continuous organic phase (FC-40 incorporating 1% surfactant). To control droplet dimensions, flow rates of the NP aqueous phase were held constant at 1 μL/min, and the organic flow rate was varied between 20 and 70 μL/min. Droplets were then deposited from the chip outlet tubing onto a silicon substrate and allowed to dry by heating the substrates to 550 °C. During the drying process, the NPs would then self-assemble into a supercluster with the diameter being governed by the initial droplet size and NP concentration (Figure 1c).

Examples of generated self-assembled colloids using sonication are shown in Figure 2a for polydisperse citrate-stabilized Ag NPs, 43 nm citrate-stabilized Au NPs (Figure 2b,c), and 16 nm Au NPs stabilized with 12-mercaptododecanoic acid (MDDA) (SI Figure S2). In both cases superclusters ranging in diameter, D, between 100 and 5000 nm could be achieved. On the other hand, examples showing the use of a microfluidic strategy have been employed to generate droplets containing 16 nm Au particles stabilized by MDDA in a partially self-assembled state (see Figure 2d). Upon evaporation of the aqueous phase, uniform monodisperse clusters ranging in diameter between 4.64 and 8.61 μm could be generated depending on flow conditions (Figure 2e,f). Using this approach the supercluster diameter was limited by the channel dimensions, pipet diameter, and flow rates. Droplet dimension is regulated by flow rate: increasing the flow rate leads to smaller droplets; a similar effect can be achieved keeping a constant flow rate but using a smaller pipet diameter. Generated droplets, thus clusters, of different sizes exhibit high regularity (SI Figure S3). Although microfluidic routes allow for unparalleled levels of control, the simplicity of sonication also has merit in the context of rapidly generating SERS-active substrates (examples of SEMs of 16 nm MDDA-functionalized Au particles are shown in SI Figure S3).

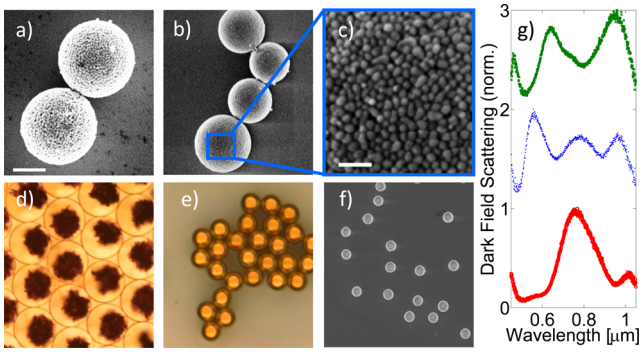

Figure 2. SEMs and optical image of colloids formed by emulsification and through microfluidics. (a) Superclusters made from polydisperse citrate-stabilized silver particles. (b, c) Superclusters made from 43 nm citrate-stabilized gold particles. (d) Microfluidic droplets containing highly concentrated 16 nm MDDA-stabilized NPs with a distribution of 100.5 ± 0.2 μm. (e) Bright field of 8.61 μm diameter superclusters. (f) SEM image of 4.64 μm diameter superclusters. Scale bar is (a) 1 μm; (b) 2 μm; (c) 100 nm; (d) 100 μm; (e) 20 μm; (f) 10 μm. (g) Typical scattering spectra of the superclusters as measured by dark-field spectroscopy with a 100× objective and 10 s integration time.

It should be noted that due to the exceptional stability of MDDA-functionalized 16 nm particles, even when dried, the particles can be redispersed in water. The redispersed particles display a red-shifted localized plasmon resonance, suggesting that some agglomerates may nevertheless exist. Despite this, the ability to redisperse these clusters with appropriately functionalized particles may open avenues for smart drug delivery; for example if the entire cluster is protected by a lipid bilayer, it could be possible to controllably disperse the particles by rupturing the bilayer (e.g., utilizing the high absorption of the clusters in the infrared allows localized heat generation).[15] The fact that the superclusters form from evaporation of the aqueous microdroplets suggests that any species that was originally dissolved in the aqueous phase will be captured within the superclusters; these species are therefore expected to also be released upon redispersion of the particles (provided that the functionality of the particles is appropriate to prevent adsorption of these species to the particles' surface). In effect, these superclusters may allow for a label-free (i.e., no affinity to the particles is required) drug delivery platform. The delivery of a high dose of particles themselves in such a manner could then be used for the dual purpose of photothermal therapy and/or contrast agents for theranostics.[43]

Unlike the spheres formed by MDDA-functionalized particles, those formed by citrate-stabilized particles do not break up in water. This fact can be advantageous, as citrate groups can be displaced from the superclusters, meaning that aqueous chemistries can be subsequently performed on them. Furthermore, the fact that the superclusters in Figure 2 are themselves formed of particles leads to a natural porosity of the structure,[44] meaning that despite the relatively large volume of the superclusters, a large portion of the surface area of the NPs is retained; this is beneficial for sensing applications such as uniform substrates for SERS. In this context, as will be shown, field enhancement or "hot spots" are generated throughout the clusters at certain wavelengths, making the total enhancement substantial compared to more conventional aggregation-based substrates.

An implication of the mechanism of the supercluster formation is that, in principle, they can be made of any nanoscopic building blocks. In other words the NPs that the spheres are composed of should not be limited by material, shape, or chemical composition of the initial aqueous phase. This assertion is supported by the fact that quite "challenging" building blocks for hierarchical assembly such as cetyltrimethy-

DOI: 10.1021/acsphotonics.5b00408
ACS Photonics 2016, 3, 35−42

lammonium bromide (CTAB)-stabilized gold nanorods (SI Figure S4), citrate-stabilized silver prisms (SI Figure S5), and a mixed sample composed of citrate-stabilized silver rods, spheres, and prisms can be assembled via this method. In the case of CTAB-stabilized nanorods, the high concentration of CTAB (0.1 M) in the NP solution means that salting out of the CTAB is occasionally observed; for example in SI Figure S4, dark regions of nonconductive CTAB-rich sections of the spheres are clearly visible. However, despite this, the formed superclusters retain their uniform spherical geometry. In the case of citrate-stabilized silver prisms (SI Figure S5) however, indentations and protrusions are observed in the morphology of the spheres. Despite these defects, the general spherical nature of the superclusters with silver prisms is apparent.

Given that any type of particle could in principle become incorporated into the superclusters means that they are a natural platform for multiplexing opportunities. For example, it is possible to incorporate magnetic particles, together with plasmonic NPs, in order to effectively obtain a particle that displays both properties (SI Figure S6); alternatively the introduction of multiple surface functionalities becomes trivial. Additionally, such structures enable a route to the synthesis of large, monodisperse particles with a wide range of compositions. If a metal salt is reduced onto the surface of the spheres, uniform spherical particles in the size range of approximately 50 nm to 5 μm can in principle be formed; for metals such as gold, the synthesis of monodisperse spherical particles of this size is highly challenging.[45]

We further characterize these superclusters by measuring their optical properties via dark-field spectroscopy,[46] from which one can extract the light scattered off micro- and nanoparticles. Typical dark-field spectra are presented in Figure 2g for three unique superclusters of varying size, where one can easily identify strong, tunable optical resonances, which will be explored and arise from the strong coupling of the constituent NPs.

In order to investigate in more detail the optical modes supported by the superclusters, finite-difference time domain simulations[47] were performed, which allowed us to access both the spectral and near-field properties of the structures. Due to their high complexity and fine details, cylindrical geometries were used, as it is well known that the electromagnetic properties of spheres can be approximated by cylinders as long as the polarization is properly considered. Here the interest is in the p-polarized incident field, as it can excite localized surface plasmons responsible for high-field enhancements, which can then be harvested for ultrasensitive molecular spectroscopy for instance. The simulated geometry is depicted in Figure 3a, consisting of an agglomerate with size D of small metallic NPs with diameter d and spaced by a gap g. In SI Figure S7 we show the normalized absorption cross-section of a large gold sphere with a size typical of one of the superclusters along with that of a dimer composed by the constituent NPs. As can be seen clearly, these two geometries support a localized surface plasmon resonance (LSPR) in the visible range, and no other modes are found at lower energies. When one assembles the nanoparticles into a colloidal supercluster such as shown in Figure 3a, the strong coupling leads to the formation of collective supermodes (see Figure 3b–d), nonexistent in the isolated or dimer geometries presented in SI Figure S7. Clearly, these modes are similar to those observed by dark-field spectroscopy, as shown in Figure 2g. From the calculations, it can be seen that they exist for good metals such as Ag, Au, and

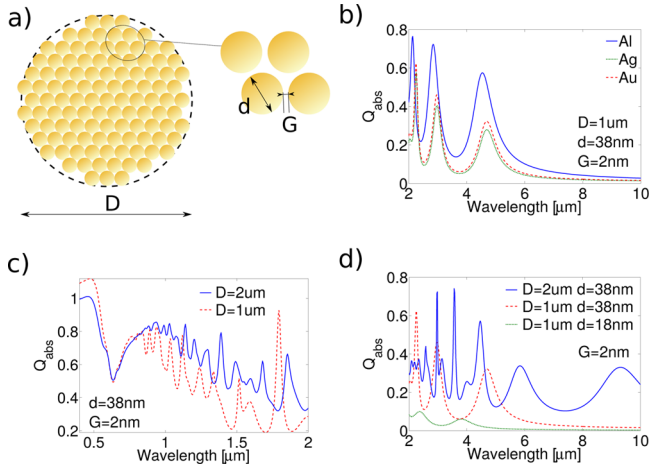

Figure 3. Absorption cross-sections of superclusters as calculated by FDTD. (a) Simulated geometry consisting of metallic nanoparticles of diameter d arranged into a large colloid cylinder with diameter D and spaced by a gap G. (b) Optical properties for a [D, d, G] = [1 μm, 38 nm, 2 nm] supercluster made out of aluminum (solid blue), silver (dotted green), and gold (dashed red). (c and d) Optical properties of a gold superclusters for G = 2 nm and various diameters in the visible and near-infrared (c) and mid-infrared (d) where [D, d] = [2 μm, 38 nm] (solid blue), [1 μm, 38 nm] (dashed red), and [1 μm, 18 nm] (dotted green).

Al (Figure 3b) and span from the visible up to 10 μm. As is usual with such resonances, one can appreciate that they become sharper and more numerous toward higher energies. In addition the modes are found to be robust and offer excellent tunability by varying gap size and nanoparticle dimensions in the whole spectral range.

To gain more insight on the light interaction within these superclusters, we look more closely at the resonances analyzing the near-field distributions. In Figure 4 we focus on the absorption of a gold supercluster (D = 2 μm) made with 38 nm gold NPs separated by 2 nm gaps. We study the near field at the peak positions shown in the absorption spectrum of Figure 4a. In particular, in Figure 4b, we show the electric field enhancement in logarithmic scale at a resonance peak (see Figure 4a), and we find an average intensity enhancement nearing 600 times the incident. Such enhancements are extremely useful in spectroscopic techniques such as SERS and SEIRA. Despite the fact that they are not record values (but quite high), we stress that they are delocalized in each gap between the NPs. This is extremely relevant to spectroscopy because large hot spot densities lead to a larger molecular cross-section in both interaction with the field and detection. It is worth mentioning that a similar enhancement is found in dimers, but now we have thousands of them localized in a cluster with a 2 μm diameter.

We now focus on the origin of these resonances. In particular, due to the large electric field enhancements between NPs, we look at the magnetic field, which is smoother. In Figure 4c,d we show the magnetic field distributions at each peak marked in Figure 4a. We can appreciate the usual field distribution (radial and angular modes) found in a transparent cylinder.[47] In other words, despite the large metallic filling fraction of the superclusters, light is found to travel inside them. These colloids thus present an effective dielectric constant that allows light to penetrate and excite a large set of optical modes in a wide frequency range. More, continuity across the two

DOI: 10.1021/acsphotonics.5b00408
ACS Photonics 2016, 3, 35–42

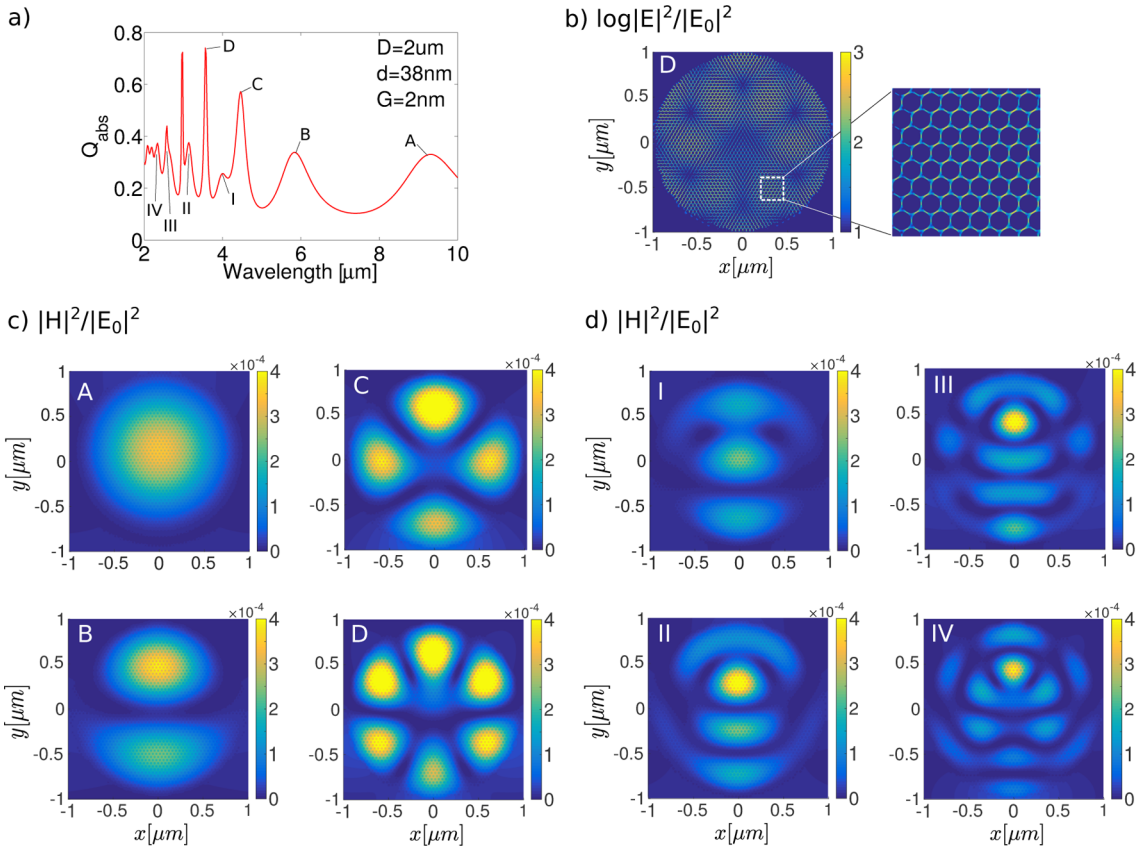

Figure 4. Collective optical supermodes of the superclusters. (a) Absorption efficiency of a gold colloid with $[D, d, G] = [2\ \mu m, 38\ nm, 2\ nm]$ with the radially and angularly quantized supermodes labeled. (b) Near-field enhancement of the electric intensity within the gaps in log scale for the fourth-order supermode, which averages at about 600 times the incident. (c and d) Magnetic field pattern for the two sets of supermodes. Note that the light is incident from the bottom.

media imposes that the electric field is mainly concentrated within the gaps.

To assess the viability of our self-assembled colloids for surface-enhanced spectroscopy, a self-limiting monolayer of MGITC was deposited on their surface. The absorption spectrum of this molecule is shown in SI Figure S8, where one can clearly identify a peak at 632.8 nm and a strong decrease in absorption beyond 650 nm. Therefore, one can expect the Raman cross-section of MGITC to be significantly enhanced at 632.8 nm compared to other excitation wavelengths with a strong fallout above 650 nm. We present in Figure 5 the SERS results of MGITC deposited on the supercluster. These spectra were generated using 532, 632.8, 685, and 785 nm lasers normalized to a power of 9 mW and collected over an exposure time of 5 s. Most strikingly, we observe that the 785 nm excitation (red dashed line) exhibits the highest Raman scattering compared to the 532 nm (solid blue) and the resonant 632.8 nm (dotted green) lines, while we had expected the latter to be the largest, followed by the 532 nm (1/10 smaller) and the 685 nm (barely measurable). We interpret these results as a clearly different electromagnetic contribution to the SERS factors at the different pump frequencies. In fact, we have calculated the electric field distributions (near-field maps) for a cluster with similar characteristics, and we can appreciate (see Figure 5c–e) important differences varying the pump frequency. In particular, thanks to the excitations of plasmonics modes, we can appreciate a poor enhancement at 532 nm, while the strongest enhancement is obtained at 785 nm. These results

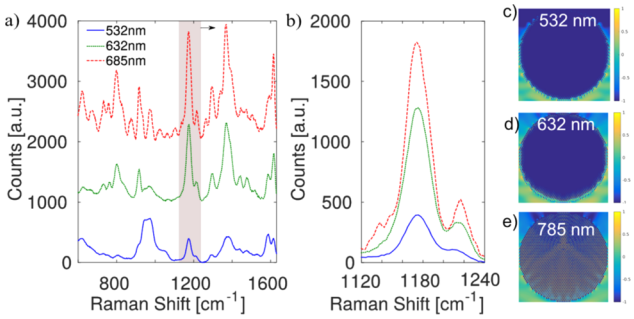

Figure 5. SERS experiments with single-layer malachite green. (a) Baseline-corrected typical Raman spectra of superclusters coated with malachite green. All three laser lines are set to equal power, and the spectra are obtained from the same colloid. (b) Zoom-in of the shaded area in (a) showing the relative strength of the 1175 cm^{-1} mode of malachite green. Note that the 632.8 nm line is resonant with this molecule. The integration time was set to 5 s with a 20× objective. (c–e) Electric field distributions (near-field maps) of similar clusters at 532, 632, and 785 nm, respectively.

complement the work of Mirkin and Schatz, where they study the optical properties of micrometer-sized superlattices and discuss the interplay between plasmons and photonic modes albeit with larger interparticle spacing.[48,49] This highlights the huge promises held by our superclusters where the strong optical resonance engineering could enable an ideal platform for ultrasensitive spectroscopy. This is reinforced by the powerful tunability offered by the synthesis method, where

DOI: 10.1021/acsphotonics.5b00408
ACS Photonics 2016, 3, 35–42

changes in material, gap, or NP size can shift appreciably the optical response.

In conclusion we have demonstrated a universal method to self-assemble superclusters in the range of 50 nm to 5 μm from (in principle) any aqueous nanoscopic building blocks using both sonication and microfluidic routes. Such superclusters open many fascinating avenues of research in nanomedicine, sensing, catalysis, and advanced materials. As an example we study the optical properties of these systems numerically and experimentally and observe strong collective supermodes in the visible and mid-IR. We then use these modes as strong hot spots in a SERS experiment where we strongly enhance the Raman cross-section of low concentrations of malachite green by over 2 orders of magnitude. We also show that due to a broad range of resonances in both the visible and infrared, the clusters can be easily tuned to the excitation wavelength of the analyte to maximize enhancement levels.

METHODS

Nanoparticle Synthesis. MDDA Au NPs of 16 nm were synthesized by the addition of either 8.62 mg (0.0219 mmol) or 17.24 mg (0.0438 mmol) of $HAuCl_4 \cdot 3H_2O$ to 95 mL of ultrapure water, followed by bringing the solution to reflux. To this was added 20 mg (0.0680 mmol) of sodium citrate dihydrate in 5 mL of ultrapure water, and the reaction proceeded to completion within 5 min, after which the heating was reduced to 60 °C and 10 mg (0.0430 mmol) of 12-mercaprododecanoic acid was added in 0.5 mL of methanol. The solution was then cooled to room temperature, and the excess unfunctionalized MDDA precipitated out and filtered through a 0.2 μm syringe filter. The resultant solution had a localized surface plasmon maximum at 525 nm and an absorbance at the maximum of 0.86. Prior to formation of the high-density solution, the NPs were concentrated by a factor of ∼10 through conventional centrifugation at 10 000 rpm (∼9000g) for 5−10 min on an Eppendorf 5424 microcentrifuge.

Citrate-stabilized Au particles of 43 nm were synthesized through a similar method to that outlined above, with the exception of the addition of 8.4 mg of sodium citrate in 5 mL and the lack of the functionalization step. The resultant particles had a localized surface plasmon maximum of 532 nm and an absorbance at the maximum of 0.80. This solution was also concentrated through centrifugation prior to high-density aqueous phase formation; however to prevent aggregation, a reduced RPM of 4000 (∼1500g) was used for 10 min.

Silver nanoparticles were made via the citrate reduction of $AgNO_3$ as described by Lee and Meisel.[50] A 36 mg (0.212 mmol) amount of $AgNO_3$ was dissolved in 190 mL of ultrapure water and brought to reflux. Following this, 10 mL of a 1% sodium citrate solution was then added to the silver solution, and reflux was allowed to continue for a further 15 min, before being allowed to cool to room temperature. The resulting silver particles were characterized by TEM imaging and were shown to be polydisperse in terms of size as well as shape (e.g., spheres, prisms, and rods). The high-density aqueous phase was formed by centrifuging this mixture at an RCF of 1500g for 10 min.

Formation of Superclusters via Sonication. The preconcentrated NP solutions (1 mL) were added to a 2 mL graduated centrifuge tube in the presence of 0.5 mL of 1,2-dichloroethane. These were then centrifuged for 5 min; for 43 nm particles an RPM of 4000 was used, while for 16 nm MDDA particles this was increased to 14 680 (∼20000g). The main bulk aqueous phase supernatant was removed by pipetting, leaving the high-density aqueous solution and DCE. This was then sonicated until the high-density phase broke off into an emulsion, and the emulsion separates back out into the two separate phases over time; therefore a 50 μL aliquot of the resulting mixture was quickly transferred onto a solid substrate for imaging and allowed to dry at room temperature.

Surface-Enhanced Raman Spectroscopic Measurements. SERS measurements were performed on a home-built Raman microscope consisting of 532, 632.8, and 685 nm excitation sources and coupled to an inverted optical microscope.[51] The light was focused onto a 50 μm entrance slit of a spectrograph (303 mm focal length, Shamrock SR-303i, Andor) coupled to an electron multiplying charge coupled device (EMCCD, Newton DU970BV, Andor).

ASSOCIATED CONTENT

Supporting Information

The Supporting Information is available free of charge on the ACS Publications website at DOI: 10.1021/acsphotonics.5b00408.

Additional figures (PDF)

AUTHOR INFORMATION

Corresponding Authors

*E-mail: s.maier@imperial.ac.uk.
*E-mail: v.giannini@imperial.ac.uk.
*E-mail: Joshua.edel@imperial.ac.uk.

Author Contributions

[§]V. A. Turek, Y. Francescato, and P. Cadinu contributed equally to this work.

Notes

The authors declare no competing financial interest.

ACKNOWLEDGMENTS

J.B.E. acknowledges the ERC for a starting investigator grant and the EPSRC for financial support. S.A.M. and V.G. acknowledges the EPRSC Reactive Plasmonics Programme (EP/M013812/1), the Leverhulme Trust, and ONR Global for funding. V.A.T. and Y.F. thank the EPSRC doctoral prize fellowship scheme for financial support.

REFERENCES

(1) Whitesides, G. M.; Grzybowski, B. Self-Assembly at All Scales. *Science* **2002**, *295*, 2418−2421.

(2) Grzelczak, M.; Vermant, J.; Furst, E. M.; Liz-Marzán, L. M. Directed Self-Assembly of Nanoparticles. *ACS Nano* **2010**, *4*, 3591−3605.

(3) Lin, Y.; Boker, A.; He, J.; Sill, K.; Xiang, H.; Abetz, C.; Li, X.; Wang, J.; Emrick, T.; Long, S.; Wang, Q.; Balazs, A.; Russell, T. P. Self-directed self-assembly of nanoparticle/copolymer mixtures. *Nature* **2005**, *434*, 55−59.

(4) Seeman, N. C. Nanomaterials based on DNA. *Annu. Rev. Biochem.* **2010**, *79*, 65−87.

(5) Warren, S. C.; Messina, L. C.; Slaughter, L. S.; Kamperman, M.; Zhou, Q.; Gruner, S. M.; DiSalvo, F. J.; Wiesner, U. Ordered Mesoporous Materials from Metal Nanoparticle−Block Copolymer Self-Assembly. *Science* **2008**, *320*, 1748−1752.

(6) Kovtyukhova, N. I.; Mallouk, T. E. Nanowires as Building Blocks for Self-Assembling Logic and Memory Circuits. *Chem. - Eur. J.* **2002**, *8*, 4354−4363.

DOI: 10.1021/acsphotonics.5b00408
ACS Photonics 2016, 3, 35−42

(7) Park, J.; Kang, E.; Son, S. U.; Park, H. M.; Lee, M. K.; Kim, J.; Kim, K. W.; Noh, H. J.; Park, J. H.; Bae, C. J.; Park, J. G.; Hyeon, T. Monodisperse Nanoparticles of Ni and NiO: Synthesis, Characterization, Self-Assembled Superlattices, and Catalytic Applications in the Suzuki Coupling Reaction. *Adv. Mater.* **2005**, *17*, 429−434.
(8) Daniel, M.-C.; Astruc, D. Gold Nanoparticles: Assembly, Supramolecular Chemistry, Quantum-Size-Related Properties, and Applications toward Biology, Catalysis, and Nanotechnology. *Chem. Rev.* **2003**, *104*, 293−346.
(9) Boker, A.; He, J.; Emrick, T.; Russell, T. P. Self-assembly of nanoparticles at interfaces. *Soft Matter* **2007**, *3*, 1231−1248.
(10) Srivastava, S.; Kotov, N. A. Nanoparticle assembly for 1D and 2D ordered structures. *Soft Matter* **2009**, *5*, 1146−1156.
(11) Turek, V. A.; Cecchini, M. P.; Paget, J.; Kucernak, A. R.; Kornyshev, A. A.; Edel, J. B. Plasmonic Ruler at the Liquid−Liquid Interface. *ACS Nano* **2012**, *6*, 7789−7799.
(12) Nykypanchuk, D.; Maye, M. M.; van der Lelie, D.; Gang, O. DNA-guided crystallization of colloidal nanoparticles. *Nature* **2008**, *451*, 549−552.
(13) Cecchini, M. P.; Turek, V. A.; Demetriadou, A.; Britovsek, G.; Welton, T.; Kornyshev, A. A.; Wilton-Ely, J. D. E. T.; Edel, J. B. Heavy Metal Sensing Using Self-Assembled Nanoparticles at a Liquid-Liquid Interface. *Adv. Opt. Mater.* **2014**, *2*, 966−977.
(14) Edel, J. B.; Kornyshev, A. A.; Urbakh, M. Self-Assembly of Nanoparticle Arrays for Use as Mirrors, Sensors, and Antennas. *ACS Nano* **2013**, *7*, 9526−9532.
(15) Brugarolas, T.; Tu, F.; Lee, D. Directed assembly of particles using microfluidic droplets and bubbles. *Soft Matter* **2013**, *9*, 9046−9058.
(16) Zhao, Y.; Shang, L.; Cheng, Y.; Gu, Z. Spherical Colloidal Photonic Crystals. *Acc. Chem. Res.* **2014**, *47*, 3632−3642.
(17) Lee, S. H.; Yu, S.-H.; Lee, J. E.; Jin, A.; Lee, D. J.; Lee, N.; Jo, H.; Shin, K.; Ahn, T.-Y.; Kim, Y.-W.; Choe, H.; Sung, Y.-E.; Hyeon, T. Self-Assembled Fe3O4 Nanoparticle Clusters as High-Performance Anodes for Lithium Ion Batteries via Geometric Confinement. *Nano Lett.* **2013**, *13*, 4249−4256.
(18) Zhao, X.; Cao, Y.; Ito, F.; Chen, H.-H.; Nagai, K.; Zhao, Y.-H.; Gu, Z.-Z. Colloidal Crystal Beads as Supports for Biomolecular Screening. *Angew. Chem., Int. Ed.* **2006**, *45*, 6835−6838.
(19) Gu, H.; Rong, F.; Tang, B.; Zhao, Y.; Fu, D.; Gu, Z. Photonic Crystal Beads from Gravity-Driven Microfluidics. *Langmuir* **2013**, *29*, 7576−7582.
(20) Wu, L. M.; Shen, Z. H.; Zhu, Y.; You, B.; Zi, J. Fabrication of Robust Crystal Balls from the Electrospray of Soft Polymer Spheres/Silica Dispersion. *Langmuir* **2010**, *26*, 6604−6609.
(21) Guo, J.; Yang, W.; Wang, C. Magnetic colloidal supraparticles: design, fabrication and biomedical applications. *Adv. Mater.* **2013**, *25*, 5196−5214.
(22) Boal, A. K.; Ilhan, F.; DeRouchey, J. E.; Thurn-Albrecht, T.; Russell, T. P.; Rotello, V. M. Self-assembly of nanoparticles into structured spherical and network aggregates. *Nature* **2000**, *404*, 746−748.
(23) Geyer, T.; Born, P.; Kraus, T. Switching Between Crystallization and Amorphous Agglomeration of Alkyl Thiol-Coated Gold Nanoparticles. *Phys. Rev. Lett.* **2012**, *109*, 128302.
(24) Lacava, J.; Born, P.; Kraus, T. Nanoparticle Clusters with Lennard-Jones Geometries. *Nano Lett.* **2012**, *12*, 3279−3282.
(25) Galván-Moya, J. E.; Altantzis, T.; Nelissen, K.; Peeters, F. M.; Grzelczak, M.; Liz-Marzán, L. M.; Bals, S.; Van Tendeloo, G. Self-Organization of Highly Symmetric Nanoassemblies: A Matter of Competition. *ACS Nano* **2014**, *8*, 3869−3875.
(26) Sánchez-Iglesias, A.; Grzelczak, M.; Altantzis, T.; Goris, B.; Pérez-Juste, J.; Bals, S.; Van Tendeloo, G.; Donaldson, S. H.; Chmelka, B. F.; Israelachvili, J. N.; Liz-Marzán, L. M. Hydrophobic Interactions Modulate Self-Assembly of Nanoparticles. *ACS Nano* **2012**, *6*, 11059−11065.
(27) Grzelczak, M.; Sánchez-Iglesias, A.; Liz-Marzán, L. M. Solvent-induced division of plasmonic clusters. *Soft Matter* **2013**, *9*, 9094−9098.
(28) Singh, G.; Chan, H.; Baskin, A.; Gelman, E.; Repnin, N.; Král, P.; Klajn, R. Self-assembly of magnetite nanocubes into helical superstructures. *Science* **2014**, *345*, 1149−1153.
(29) Turek, V. A.; Elliott, L. N.; Tyler, A. I. I.; Demetriadou, A.; Paget, J.; Cecchini, M. P.; Kucernak, A. R.; Kornyshev, A. A.; Edel, J. B. Self-Assembly and Applications of Ultraconcentrated Nanoparticle Solutions. *ACS Nano* **2013**, *7*, 8753−8759.
(30) Cho, Y.-S.; Yi, G.-R.; Kim, S.-H.; Pine, D. J.; Yang, S.-M. Colloidal Clusters of Microspheres from Water-in-Oil Emulsions. *Chem. Mater.* **2005**, *17*, 5006−5013.
(31) Edel, J. B.; Fortt, R. Microfluidic routes to the controlled production of nanoparticles. *Chem. Commun.* **2002**, 1136−1137.
(32) Gong, X. Q.; Patil, A. V.; Ivanov, A. P.; Kong, Q. Y.; Gibb, T.; Dogan, F.; deMello, A. J.; Edel, J. B. Label-Free In-Flow Detection of Single DNA Molecules using Glass Nanopipettes. *Anal. Chem.* **2014**, *86*, 835−841.
(33) Cecchini, M. P.; Stapountzi, M. A.; McComb, D. W.; Albrecht, T.; Edel, J. B. Flow-Based Autocorrelation Studies for the Detection and Investigation of Single-Particle Surface-Enhanced Resonance Raman Spectroscopic Events. *Anal. Chem.* **2011**, *83*, 1418−1424.
(34) de Nijs, B.; Dussi, S.; Smallenburg, F.; Meeldijk, J. D.; Groenendijk, D. J.; Filion, L.; Imhof, A.; van Blaaderen, A.; Dijkstra, M. Entropy-driven formation of large icosahedral colloidal clusters by spherical confinement. *Nat. Mater.* **2015**, *14*, 56−60.
(35) Soukoulis, C. M.; Wegener, M. Past achievements and future challenges in the development of three-dimensional photonic metamaterials. *Nat. Photonics* **2011**, *5*, 523−530.
(36) Giannini, V.; Fernandez-Dominguez, A. I.; Heck, S. C.; Maier, S. A. Plasmonic nanoantennas: fundamentals and their use in controlling the radiative properties of nanoemitters. *Chem. Rev.* **2011**, *111*, 3888−3912.
(37) Paniagua-Domínguez, R.; Abujetas, D. R.; Sánchez-Gil, J. A. Ultra low-loss, isotropic optical negative-index metamaterial based on hybrid metal-semiconductor nanowires. *Sci. Rep.* **2013**, *3*, 1507.
(38) Rockstuhl, C.; Lederer, F.; Etrich, C.; Pertsch, T.; Scharf, T. Design of an artificial three-dimensional composite metamaterial with magnetic resonances in the visible range of the electromagnetic spectrum. *Phys. Rev. Lett.* **2007**, *99*, 017401.
(39) Huebner, A.; Sharma, S.; Srisa-Art, M.; Hollfelder, F.; Edel, J. B. Microdroplets: a sea of applications? *Lab Chip* **2008**, *8*, 1244−1254.
(40) Solvas, X. C. I.; Srisa-Art, M.; Demello, A. J.; Edel, J. B. Mapping of Fluidic Mixing in Microdroplets with 1 mu s Time Resolution Using Fluorescence Lifetime Imaging. *Anal. Chem.* **2010**, *82*, 3950−3956.
(41) Srisa-Art, M.; deMello, A. J.; Edel, J. B. High-throughput DNA droplet assays using picoliter reactor volumes. *Anal. Chem.* **2007**, *79*, 6682−6689.
(42) Gibb, T. R.; Ivanov, A. P.; Edel, J. B.; Albrecht, T. Single Molecule Ionic Current Sensing in Segmented Flow Microfluidics. *Anal. Chem.* **2014**, *86*, 1864−1871.
(43) Janib, S. M.; Moses, A. S.; MacKay, J. A. Imaging and drug delivery using theranostic nanoparticles. *Adv. Drug Delivery Rev.* **2010**, *62*, 1052−1063.
(44) Velev, O. D.; Jede, T. A.; Lobo, R. F.; Lenhoff, A. M. Porous silica via colloidal crystallization. *Nature* **1997**, *389*, 447−448.
(45) Kimling, J.; Maier, M.; Okenve, B.; Kotaidis, V.; Ballot, H.; Plech, A. Turkevich Method for Gold Nanoparticle Synthesis Revisited. *J. Phys. Chem. B* **2006**, *110*, 15700−15707.
(46) Lei, D. Y.; Appavoo, K.; Sonnefraud, Y.; Haglund, R. F.; Maier, S. A. Single-particle plasmon resonance spectroscopy of phase transition in vanadium dioxide. *Opt. Lett.* **2010**, *35*, 3988−3990.
(47) Huffman, C. F. B. a. D. R. *Absorption and Scattering of Light by Small Particles*; Wiley Interscience: New York, 1983.
(48) Ross, M. B.; Blaber, M. G.; Schatz, G. C. Using nanoscale and mesoscale anisotropy to engineer the optical response of three-dimensional plasmonic metamaterials. *Nat. Commun.* **2014**, *5*, 4090.
(49) Ross, M. B.; Ku, J. C.; Vaccarezza, V. M.; Schatz, G. C.; Mirkin, C. A. Nanoscale form dictates mesoscale function in plasmonic DNA-nanoparticle superlattices. *Nat. Nanotechnol.* **2015**, *10*, 453−458.

DOI: 10.1021/acsphotonics.5b00408
ACS Photonics 2016, 3, 35−42

(50) Lee, P. C.; Meisel, D. Adsorption and surface-enhanced Raman of dyes on silver and gold sols. *J. Phys. Chem.* **1982**, *86*, 3391−3395.
(51) Crick, C. R.; Albella, P.; Ng, B.; Ivanov, A. P.; Roschuk, T.; Cecchini, M. P.; Bresme, F.; Maier, S. A.; Edel, J. B. Precise attoliter temperature control of nanopore sensors using a nanoplasmonic bullseye. *Nano Lett.* **2015**, *15*, 553−559.

DOI: 10.1021/acsphotonics.5b00408
ACS Photonics 2016, 3, 35−42